University of Padua - Department of Physics and Astronomy
Course: Physics Laboratory
Academic year: 2021-22

Group 13
Vittoria Pavanello - 2055706 - vittoria.pavanello@studenti.unipd.it
Riccardo Triozzi - 2055705 - riccardo.triozzi@studenti.unipd.it
Nicola Zancopè - 2053347 - nicola.zancope@studenti.unipd.it

Laboratory days: 24-26/11/2021

Measurement of Environmental Radiation
with gamma spectroscopy techniques

Contents

1 Introduction

The aims of this experiment are:

1. to characterize two types of gamma detectors (a NaI detector and a HPGe one) through the analysis of spectra of known sources and through an estimation of the detectors' intrinsic efficiency;
2. to study the spectrum and the activity of some organic and inorganic samples exploiting the two detectors;
3. to determine the Radon's activity in a room of the "Polo didattico" building.

1.1 Experimental setup

The experimental setup exploited for the environmental radiation measurements is represented by a shielded well to which two detectors for gamma spectroscopy are connected. One of these consists of a cylindrical NaI(Tl) detector (height and diameter of 7.5 cm) placed at the bottom of the well; the other one is an Hyper-Pure Germanium (HPGe) detector maintained at fixed cryogenic temperature (the cooling down process is supplied by a liquid nitrogen dewar that covers the whole detector) and positioned on the side surface of the well itself.
The two detectors operate at the fixed voltage of HV = +700 V and HV = −2000 V respectively. The NaI(Tl) detector is coupled to a PMT: the signal is obtained from the anode and preamplified. The HPGe detector's signal is directed to a FET plus feedback network placed in the same vacuum chamber of the HPGe itself. The derived signal is successively preamplified (one of the two outputs of the preamplifier is introduced to the CAEN digitizer to obtain the energy acquisitions). Finally, a trapezoidal filter is applied to both the HPGe's and NaI(Tl) preamplified signals.

Setting of trapezoidal filter As just mentioned, a trapezoidal filter has to be imposed to the detectors' preamplified signal, aiming at removing as much as possible the electronic noise. It is obtained as a convolution of the considered signal with a proper kernel in order to transform the exponential input in an infinite exponential cusp (this shape is suitably chosen to minimize the relative noise). Exploiting the VERDI software it has been possible to properly adjust 5 parameters to optimize the filter: trigger threshold, decay time, trapezoid rise time, trapezoid flat top, trapezoid rescaling. All the parameters have been chosen in order to obtain the best resolution for a reference peak within a ^{60}Co spectrum. The chosen parameters are presented in Table 1 [1].

Parameters	**NaI(Tl)**	**HPGe**
Trigger threshold	100	200
Decay time	24000	5000
Trapezoid rise time	200	500
Trapezoid flat top	100	100
Trapezoid rescaling	20	19

Table 1: Trapezoidal parameters set

2 Characterization of the detectors

Once the digital filters are correctly set, it is possible to calibrate the two detectors. For this purpose, a source of ^{60}Co and ^{241}Am were used (the ^{22}Na source was not available). Placing each source at $d_{\text{HPGe}} = 200$ mm from the Germanium detector, the spectra were acquired for roughly 10 minutes each. Afterwards, a gaussian (plus a linear background) fit is performed for each peak of the spectra, in order to get the centroids' positions. The procedure, applied to both the detectors, is depicted in Figure 1, with fit's parameters in Table 2.
The χ^2 test is satisfactory for every fit except for the Americium one in the NaI(Tl) detector; looking at the picture (Figure 1), in fact, one can observe the high shoulder at the left of peak, probably due to Compton photons exiting the detector right after the scattering causing a partial energy deposit. Nevertheless, since we're interested only in the centroid position for calibration purpose, the fit is performed only in a part of the peak's spectrum as depicted. Seeming the mean of the function in good correspondance with the one of the data, the fitting procedure can be considered as satisfactory as the other ones.

[1] The threshold has been set at higher values for the ^{60}Co acquisition

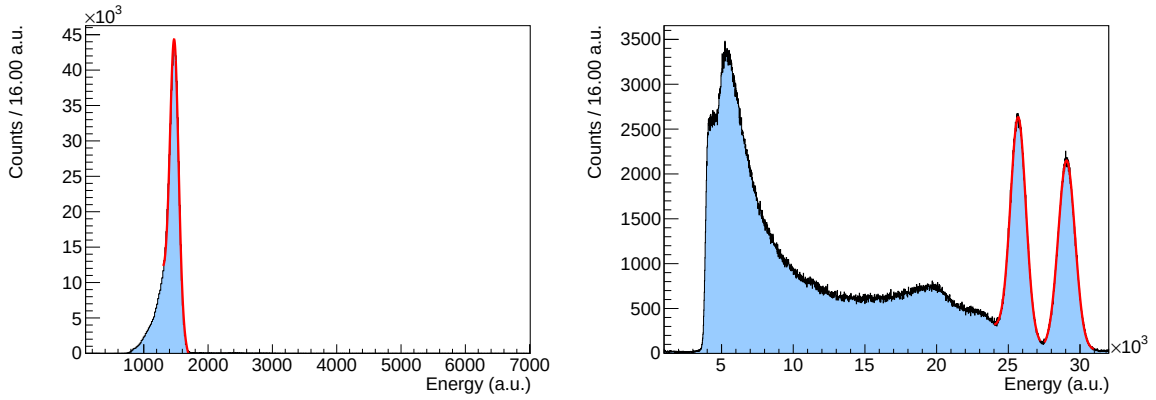

(a) ^{241}Am source, NaI(Tl) detector

(b) ^{60}Co source, HPGe detector

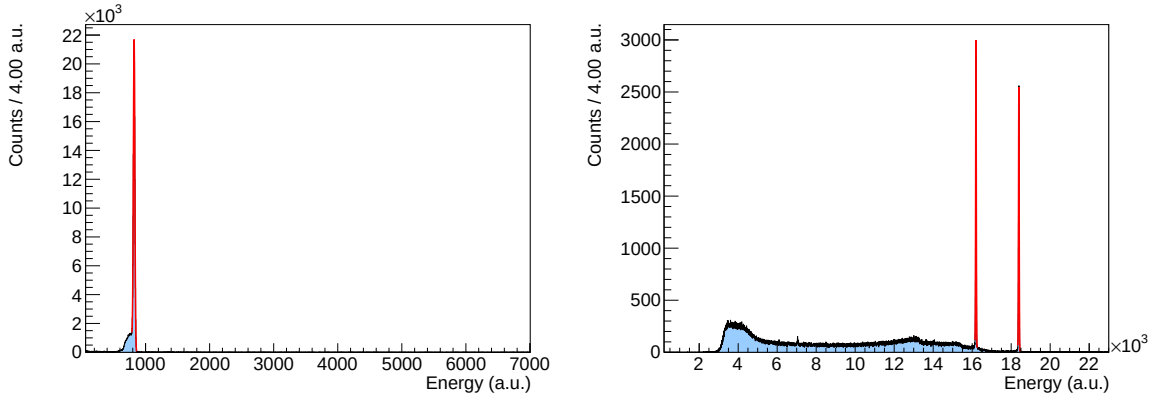

(c) ^{241}Am source, HPGe detector

(d) ^{60}Co source, HPGe detector

Figure 1: Uncalibrated spectra and relative gaussian fit.

Detector	Peak (keV)	E (a.u.)	σ (a.u.)	$\chi^2/d.o.f.$
NaI(Tl)	60	1475.1 ± 0.2	65.4 ± 0.2	49
	1173	25690 ± 2	534 ± 2	1.1
	1332	29066 ± 2	585 ± 2	0.96
HPGe	60	821.30 ± 0.04	11.4 ± 0.03	1.7
	1173	16194.4 ± 0.1	15.8 ± 0.1	2.5
	1332	18393.4 ± 0.1	16.6 ± 0.1	3.9

Table 2: Fitting parameters for the three peaks in the spectra for each of the detectors.

The centroids can be then associated with the known value of the energy for each gamma transition (60 keV, 1173 keV and 1332 keV)[2] to carry out a linear fit in order to obtain the calibration curve for each of the detectors; the procedure is depicted in Figure 2, while the final linear coefficients for the detectors are presented in Table 3.

It's difficult to establish whether a three-point linear fit is satisfactory, since the residuals cannot show possible systematic trends. What's more, the χ^2 test is not really reliable since the errors on the known value of energies are really small; in fact, $\chi^2/d.o.f. \gg 1$ for the NaI(Tl), while the HPGe's test is closer to 1, but still not completely satisfactory. Nevertheless, no problem arised in the subsequent analysis, so the calibration parameters can be accepted.

	q (keV)	m ($\frac{\text{keV}}{\text{a.u.}}$)
NaI(Tl)	-8.420 ± 0.009	0.046070 ± 0.000002
HPGe	0.043 ± 0.003	0.0724436 ± 0.0000004

Table 3: Calibration parameters for the two detectors (line equation: $y = q + mx$)

[2]The precise values are $E(^{241}\text{Am}) = 59.5409 \pm 0.0001$ keV, $E_1(^{60}\text{Co}) = 1173.228 \pm 0.003$ keV and $E_2(^{60}\text{Co}) = 1332.492 \pm 0.004$ keV. Source: http://www.nucleide.org

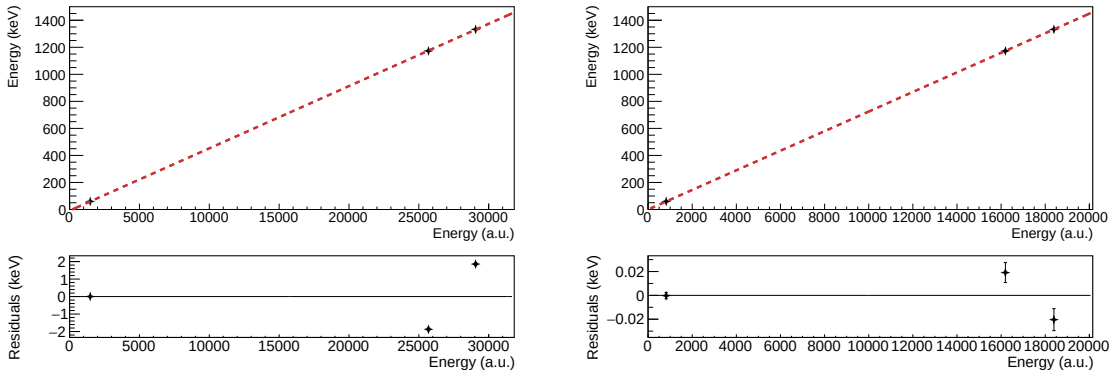

Figure 2: Calibration curves for the NaI(Tl) (left) and HPGe (right)

Resolution It is worth noting the big difference in resolution between the two detectors. In particular, defining the resolution as $R = \frac{FWHM}{E_\gamma}$, the resolution for the three peaks just analyzed are listed in Table 4. It can be easily seen that the HPGe has a way better resolution, making it suitable for the analysis that this experiment requires.

	60 keV	1173 keV	1332 keV
NaI(Tl)	12%	5.0%	4.7%
HPGe	3%	0.2%	0.2%

Table 4: Resolution for the two detectors

2.1 Intrinsic efficiency of the detectors

The measurements used to deduce the calibration of the two detectors might also be exploited to derive their intrinsic efficiency. The intrinsic efficiency ϵ_{int} is defined as the fraction of particles (photons) that are revealed by the detector with respect to the total number of particles that hit it. The first quantity coincides with the number of recorded events while the second one can be obtained knowing the source activity $\mathcal{A}$ and the solid angle covered by the detector Ω.
In order to perform an easier estimation of the angle Ω described by the detectors, two different positions were chosen to acquire the sources' spectra. For the HPGe the sources were positioned in front of the detector opening at a distance of $d_{\text{HPGe}} = 200$ mm, inside the shield itself. For the NaI(Tl) the sources were placed on top of a supporting stick distancing $d_{\text{NaI}} = 285$ mm from the center of the detector's surface. The sources included for these acquisitions were ^{60}Co and ^{241}Am.
Once recorded these measurements, one can compute ϵ_{int}. In this case it's interesting to evaluate the intrinsic efficiency referred to each full-energy peak recorded, considering the number of events relative to a specific peak (N_{peak}) as the total number of γ revealed by a detector.
The value N_{peak} was obtained as the area between a gaussian fit applied to the peak and the linear background. A graphic representation of the fits performed is depicted in Figure 3 in which both an exemplar gaussian and linear fit are carried out.

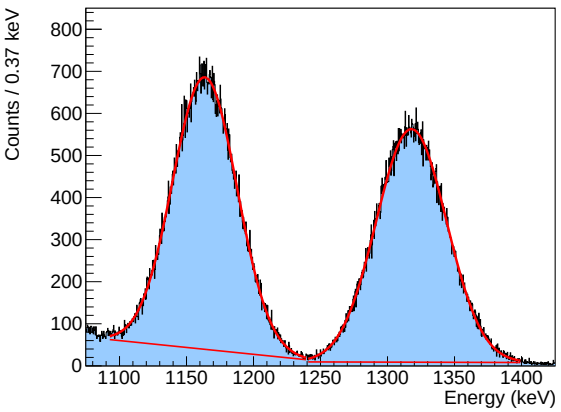

Figure 3: Graphic representation of N_{peak}: the two peaks in ^{60}Co spectrum are considered for NaI(Tl) detector.

The number of photons hitting the detector is:

$$N_{\text{in}} = \mathcal{A} \cdot \Delta t \cdot \frac{\Omega}{4\pi} \cdot P_\gamma \qquad (1)$$

in which $\mathcal{A}$ is the activity of a specific source and is deduced from tabulated values[3]; Δt is the time duration of the spectrum acquisition; Ω is the solid angle covered by the detector ($\Omega = \frac{A}{d^2}$, where A is

[3]Source: http://www.dfa.unipd.it/fileadmin/servtec/Sorgenti_polo_sett_2021_01.pdf.

the area covered by the detector with $A_{NaI} = 4418$ mm^2, $A_{HPGe} = 1200$ mm^2 and d its distance from the source); P_γ is the fraction of decays that produces a given gamma transition[4].
The results are presented in Table 5; the trend of the intrinsic efficiencies as function of gamma energy is depicted in Figure 4.

Detector	Peak (keV)	Intrinsic efficiency
NaI(Tl)	60	0.77
	1173	0.21
	1333	0.20
HPGe	60	1.02
	1173	0.16
	1333	0.15
	40	0.62
	46	0.69
	245	0.79
	344	0.57
	411	0.40
	779	0.27
	867	0.27
	964	0.23
	1112	0.20
	1408	0.16

Table 5: Intrinsic efficiencies of full-energy peaks recorded in both calibration sources' spectra and ^{152}Eu spectrum (highlighted quantities). Reference energies' peaks are referred to expected values.

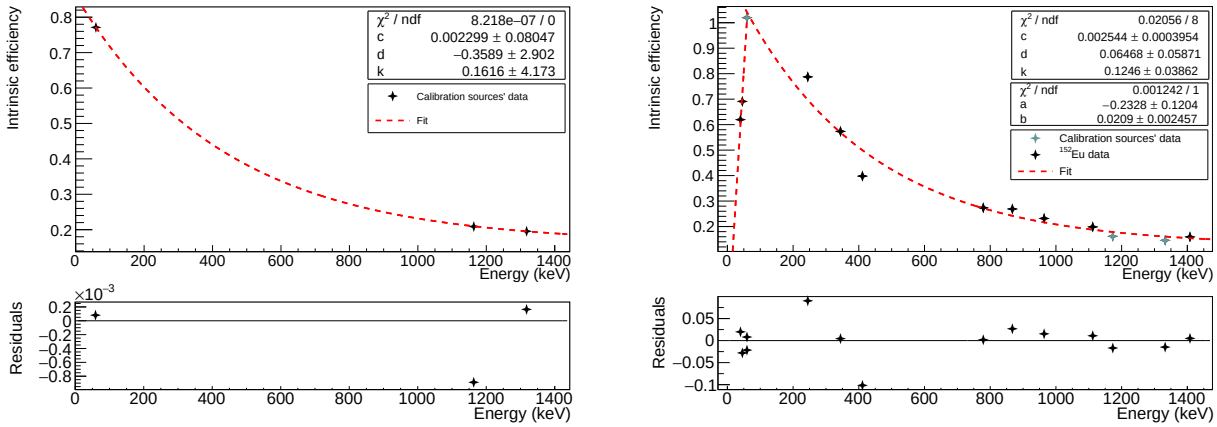

Figure 4: Intrinsic efficiency of full-energy peak trend for NaI(Tl) and HPGe detectors respectively. In the HPGe plot ^{152}Eu data are included which derivation will be presented in next Section 2.2

For what concerns the HPGe detector plot showed, it must be highlighted that Figure 4 also displays the intrinsic efficiencies associated to the photo-peaks of an additional source, ^{152}Eu. The spectrum of this source will be analyzed in the next section (Section 2.2) but it was useful to include additional data to better evaluate the trend followed by ϵ_{int}.
It is also reported that one experimental intrinsic efficiency related to HPGe detector occurs to be > 1. This result is associated to ^{241}Am peak and clearly seems unphysical (it would imply more photons recorded than the ones hitting the detector for that specific gamma transition). The explanation behind this value can be linked to the presence of events' accumulation on the left shoulder of the peak, as already observed in Section 2. Due to this left shoulder, it's probable that the corresponding N_{peak} and the intrinsic efficiency are both overestimated.
An exponential fit was applied to intrinsic efficiencies of both NaI and HPGe detectors: the fitting

[4]This quantity is estimated evaluating the photons produced per 100 disintegrations. Source: http://www.nucleide.org

function considered is $y = k + \exp(-cx + d)$. In the case of hyper-pure germanium detector it has also been introduced a linear regression at low energies to better suit the data, according to a general expression $y = a + bx$.
All the fits performed can be considered quite satisfactory, both in terms of the residuals trend (there seem not to be any systematic trend) and in term of the χ^2 test applied. It must be observed that the calculated parameters are associated to errors bigger than the parameters themselves: this apparent discrepancy might be explained noticing that all the parameters are noticeably small. Despite this consideration, the fitted functions allow to sufficiently describe the data trend and to eventually derive one detector's intrinsic efficiency at a fixed energy value.

2.2 Relative efficiency using ^{152}Eu

In addition to the previous observations on the intrinsic efficiency of the detectors it's possible to integrate further comments on the characterization of HPGe detector's efficiency. To better investigate this aspect a spectrum acquisition of ^{152}Eu has been carried out (the recorded spectrum is presented in Figure 5). The source have been placed in front of the hyper-pure germanium detector opening at distance $d_{\text{HPGe}} = 200$ mm, as already described in previous Section 2.1. The ^{152}Eu source decays both $\beta+$ and $\beta-$ to two distinct nuclei (^{152}Gd and ^{152}Sm), producing a significant number of gamma transitions. Since the relative intensities of these transitions are known, one can derive the relative efficiency trend associated to the hyper-pure germanium detector itself.

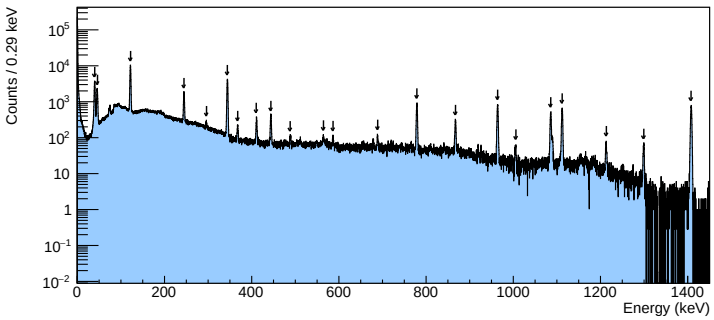

Figure 5: ^{152}Eu spectrum acquired with HPGe spectrum.

As first step a research of the energies associated to the recorded peaks has been performed. The energies are derived as the mean of a gaussian fit applied to the calibrated peaks; similarly to what presented in Section 2, the gaussian curve has been added to a linear function in order to also describe the baseline trend. The resulting parameters of these fits are summarized in Table 6.

E_{theor} (keV)	E_{fit} (keV)	σ_{fit} (keV)
40	39.83 ± 0.01	0.942 ± 0.009
46	45.54 ± 0.01	1.03 ± 0.02
122	121.768 ± 0.004	0.886 ± 0.004
245	244.72 ± 0.02	0.93 ± 0.02
344	344.273 ± 0.007	0.932 ± 0.007
411	411.09 ± 0.03	0.90 ± 0.06
444	443.96 ± 0.03	0.97 ± 0.03
779	778.89 ± 0.01	1.03 ± 0.02
867	867.39 ± 0.03	1.10 ± 0.05
964	964.05 ± 0.01	1.08 ± 0.01
1112	1112.08 ± 0.02	1.07 ± 0.02
1408	1408.12 ± 0.01	1.14 ± 0.03

Table 6: Parameters of the gaussian fits applied to ^{152}Eu spectrum's peak. The mean represents an estimation of the energy associated to the gamma transition relative to the considered peak.

It has been chosen to analyze the intrinsic efficiency of every full-energy peak acquired. The followed protocol is entirely similar to that described in the previous Section 2.1, applied multiple times for each recorded peak characterized by a significant statistics. The results are collected in Table 5. It must be highlighted that the intrinsic efficiency related to the 121.8 keV peak is not included. This choice is made because the resulting value does not appear to be physical ($\epsilon_{int}^{122\text{keV}} = 1.2 > 1$) and could hardly be fitted with the other data (fit presented in Figure 4).
Exploiting these calculations on intrinsic efficiency one can also deduce the relative efficiency trend of the HPGe detector. As anticipated, the intensities of gamma transitions analyzed are known but

it has to be observed that the possessed intensities are normalized assuming that the 1408 keV transition has yielded 100%. Therefore the experimental N_{peak} (number of events relative to a specific peak) obtained, namely the areas covered by the gaussian fit applied, need to be normalized asking that $N_{peak}^{1408\text{keV}} = 100$. Once done that, all the experimental areas have been divided by the tabulated intensities. Furthermore, all the relative efficiencies for the HPGe detector have been normalized to a specific transition's one, i.e. the 121.8 keV emission. The results are depicted in Figure 6.
The first two peaks (energy of 39.9 keV and 45.7 keV) were not considered for this analysis since the tabulated data on their gamma intensity are missing.

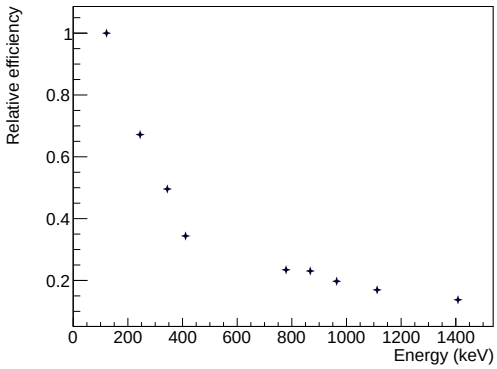

Figure 6: Relative efficiency curve of HPGe detector derived exploiting ^{152}Eu spectrum.

3 Analysis of the samples

At this point, it is possible to determine the activity of various samples by analyzing their spectra, acquired with both the detectors. The exploited samples are listed in Table 7, along with the mass m and acquisition time Δt. The activity formula can be obtained by manipulating equation (1):

$$\mathcal{A} = \frac{4\pi}{\Omega}\frac{N_{\text{in}}}{P_\gamma \Delta t} = \frac{4\pi}{\Omega P_\gamma \Delta t}\frac{N_{\text{peak}}}{\epsilon} \tag{2}$$

Sample	m (g)	t (s)
KCl	8.0 ± 0.1	1206
Pellet	193.9 ± 0.1	799
Porphyry	502.3 ± 0.1	905
ZrO_2	1870.0 ± 0.1	520

Table 7: List of samples, along with mass and acquisition time.

in which N_{in} is the number of photons that hit the detector and $N_{\text{in}} = \frac{N_{\text{peak}}}{\epsilon}$, with ϵ full-energy peak intrinsic efficiency and N_{peak} amount of events in the peak (see Section for reference 2.1). The solid angle can be calculated as $\Omega = \frac{A}{d^2}$, in which d is the distance from the source taking into account that the samples are considered point-like for the sake of this analysis. For all the samples the distance from the HPGe detector is fixed to $d_{\text{HPGe}} = 75$ mm.
In particular, regarding the NaI(Tl) detector, in the first part of the experiment the full-energy peaks intrinsic efficiencies linked to various energies were computed with the ^{60}Co and ^{241}Am sources (Section 2.1). By using the resulting efficiency versus energy relation $\epsilon(E_\gamma)$, it is possible to predict the $\epsilon_i = \epsilon(E_{\gamma_i})$ value for each identified peak[5] with energy E_{γ_i} and therefore compute N_{in}. In this way, the activity $\mathcal{A}_i$ related to each radionuclide identified in the sample is derived and the overall sample activity is $\mathcal{A} = \sum_i \mathcal{A}_i$, which can then be linked to the mass m by computing $\mathcal{A}_m := \frac{\mathcal{A}}{m}$.
For what concerns the HPGe detector, in addition to the ^{60}Co and ^{241}Am sources, the relative efficiency curve measured with the ^{152}Eu source is available (Section 2.2). The relative efficiencies can be normalized to the absolute efficiencies in order to predict the $\epsilon(E_{\gamma_i})$ values and derive the activity. Note that in practice it is only possible to roughly estimate the values for the solid angle Ω and the efficiency ϵ_i and therefore this analysis turns out to be mostly qualitative.

[5]Radionuclides were identified thanks to http://www.nucleide.org/ and the tool retrieved in http://nucleardata.nuclear.lu.se/toi/radSearch.asp

3.1 Determination of the activity

Firstly, the background was subtracted from the samples' spectra taking into account the acquisition times difference ($t_{\text{bg}} = 1686$ s). In this way, it was possible to isolate the energy peaks and thus identify the presence of a given radionuclide. The background spectra are depicted in Figure 7: the most evident peak is the ^{40}K one.

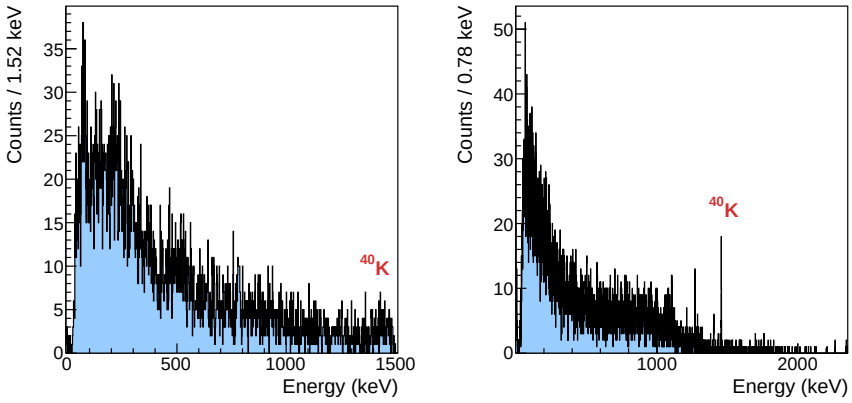

Figure 7: Background spectra linked to the NaI(Tl) (left) and HPGe (right) detectors.

KCl The first considered sample is the KCl. The background was properly removed and the only meaningful peak resulted the ^{40}K one: all the activity of the sample seems attributable to this nuclide. The spectra related to both the detectors are shown in Figure 8, focusing on the peak. It is worth noting that the HPGe is less efficient than the NaI(Tl) and the acquisition time was not lenghty enough to achieve a satisfactory statistics in the HPGe case: as a result, the interpolation and the derived activity may not be optimal. In order to compute the solid angle and use equation (2) the distance from the source is estimated to be $d_{\text{NaI}} = 20$ mm, considering that the sample was small and resting on the bottom of the container. The analysis results are listed in Table 8.

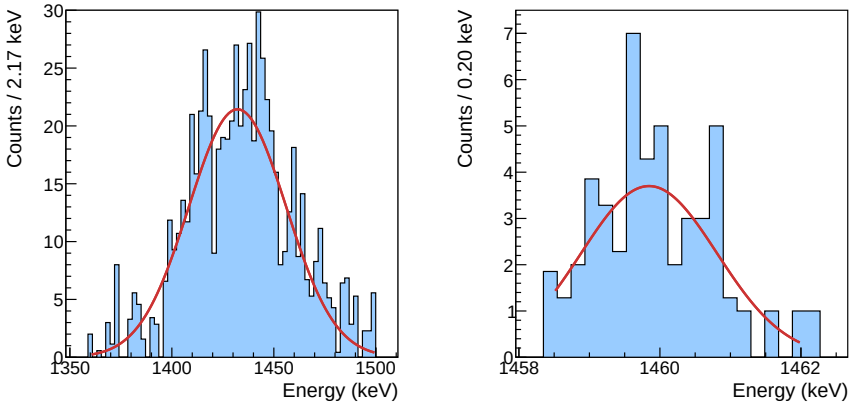

Figure 8: KCl spectra linked to the NaI(Tl) (left) and HPGe (right) detectors.

Transition (keV)	Nuclide	E_γ (keV)	N_{peak}	P_γ	$\mathcal{A}_m$ (Bq/g)
		NaI(Tl)			
1461	^{40}K	1432 ± 1	670 ± 30	0.11	4.91
		HPGe			
1461	^{40}K	1459.9 ± 0.2	48 ± 7	0.11	15.0

Table 8: Determination of the KCl sample activity.

One can observe that the activity linked to the HPGe detector is higher than the NaI(Tl) one: this will occur systematically throughout the experiment. This could be attributed to slightly unfit estimates

of the solid angle and of the efficiency: in the latter case, the value depends on a not completely satisfactory exponential fit.

Porphyry The second presented sample is the porphyry. The spectra are shown in Figure 9. Given the extension of the sample, in order to consider it as point-like in the analysis, the distance from the NaI(Tl) detector was estimated to be $d_{\mathrm{NaI}} = 37.5$ mm, taking into account in this case half the height of the sample containers ($h = 55$ mm). The analysis results are listed in Table 9: once again the statistics was not sufficient for the HPGe detector and the results may not be optimal.

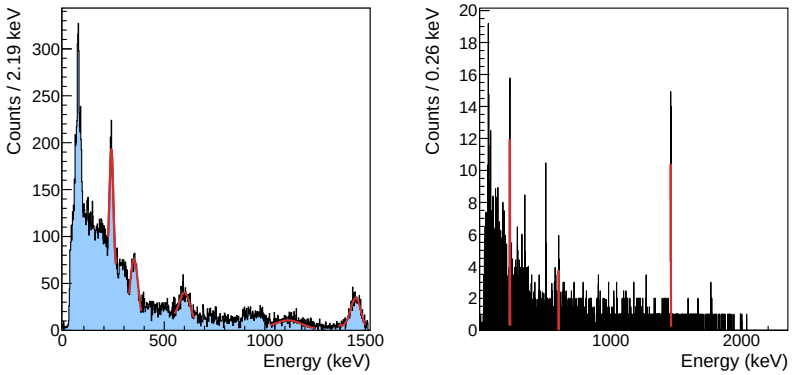

Figure 9: Porphyry spectra linked to the NaI(Tl) (left) and HPGe (right) detectors.

Transition (keV)	Nuclide	E_γ (keV)	N_{peak}	P_γ	$\mathcal{A}_m$ (Bq/g)
		NaI(Tl)			
239	^{212}Pb	237 ± 1	1280 ± 40	0.44	0.044
352	^{214}Pb	349 ± 6	1240 ± 40	0.36	0.078
609	^{214}Bi	602 ± 3	980 ± 30	0.45	0.049
1120	^{214}Bi	1120 ± 10	810 ± 30	0.15	0.221
1461	^{40}K	1453 ± 2	1030 ± 30	0.11	0.582
		HPGe			
239	^{212}Pb	231.00 ± 0.08	74 ± 9	0.44	0.033
609	^{214}Bi	602.8 ± 0.1	22 ± 5	0.45	0.018
1461	^{40}K	1457.6 ± 0.1	87 ± 9	0.11	1.30

Table 9: Determination of the porphyry sample activity.

The resulting activities are $\mathcal{A}_m^{\mathrm{NaI(Tl)}} = 0.973$ Bq/g and $\mathcal{A}_m^{\mathrm{HPGe}} = 1.35$ Bq/g.

Pellet Moreover, a sample of 'Naturkraft' pellet is presented. Once the background was properly subtracted, the spectra (see Figure 10 in Appendix for reference) did not show any evident sign of radioactive activity, maybe due to the low statistics.

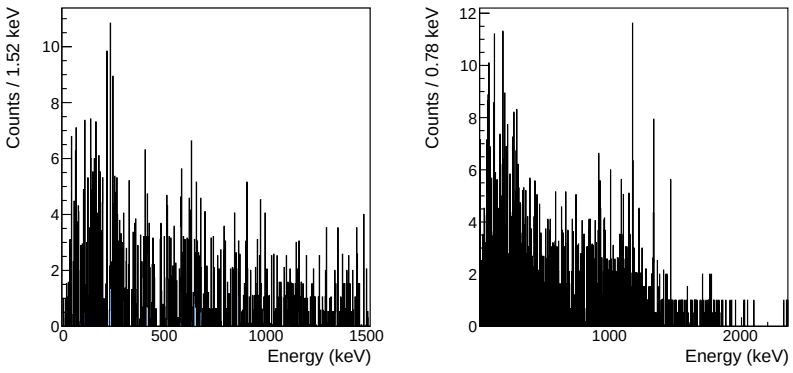

Figure 10: Pellet spectra linked to the NaI(Tl) (left) and HPGe (right) detectors.

ZrO_2 Finally, a sample of Zirconium Oxide (ZrO_2) was analyzed. The spectra are depicted in Figure 11. The distance from the Nai(Tl) is estimated to be $d_{\mathrm{NaI}} = 37.5$ mm. The results are shown in Table 10. The sample activities are $\mathcal{A}_m^{\mathrm{NaI(Tl)}} = 13.5$ Bq/g and $\mathcal{A}_m^{\mathrm{HPGe}} = 22.7$ Bq/g.

Transition (keV)	Nuclide	E_γ (keV)	N_{peak}	P_γ	$\mathcal{A}_m$ (Bq/g)
		NaI(Tl)			
186	^{226}Ra	185 ± 1	8580 ± 90	0.04	1.59
239	^{212}Pb	239.4 ± 0.4	17500 ± 100	0.44	0.281
295	^{214}Pb	295.2 ± 0.3	26500 ± 200	0.18	1.07
352	^{214}Pb	351.2 ± 0.2	50800 ± 200	0.36	1.14
609	^{214}Bi	607.5 ± 0.2	43900 ± 200	0.45	1.03
768	^{214}Bi	772 ± 3	6040 ± 80	0.05	1.59
832	^{211}Pb	834.9 ± 0.6	2740 ± 50	0.04	1.08
1120	^{214}Bi	1111.1 ± 0.6	9200 ± 100	0.15	1.17
1238	^{214}Bi	1226 ± 5	4990 ± 70	0.06	1.84
1377	^{214}Bi	1371 ± 1	4320 ± 70	0.04	2.76
		HPGe			
186	^{226}Ra	178.13 ± 0.07	1160 ± 30	0.036	2.70
295	^{214}Pb	287.59 ± 0.04	2470 ± 50	0.18	1.34
352	^{214}Pb	344.50 ± 0.03	4370 ± 70	0.36	1.35
511	^{208}Tl	508.0 ± 0.1	550 ± 20	0.23	0.351
570	^{207}Bi	576.53 ± 0.08	650 ± 30	0.98	0.109
609	^{214}Bi	602.90 ± 0.02	3880 ± 60	0.45	1.46
768	^{214}Bi	762.38 ± 0.09	410 ± 20	0.05	1.87
934	^{214}Bi	928.7 ± 0.1	250 ± 20	0.03	2.43
1120	^{214}Bi	1115.69 ± 0.05	880 ± 30	0.15	2.41
1238	^{214}Bi	1234.19 ± 0.09	330 ± 20	0.06	2.87
1764	^{214}Bi	1762.61 ± 0.05	720 ± 30	0.15	5.79

Table 10: Determination of the ZrO_2 sample activity.

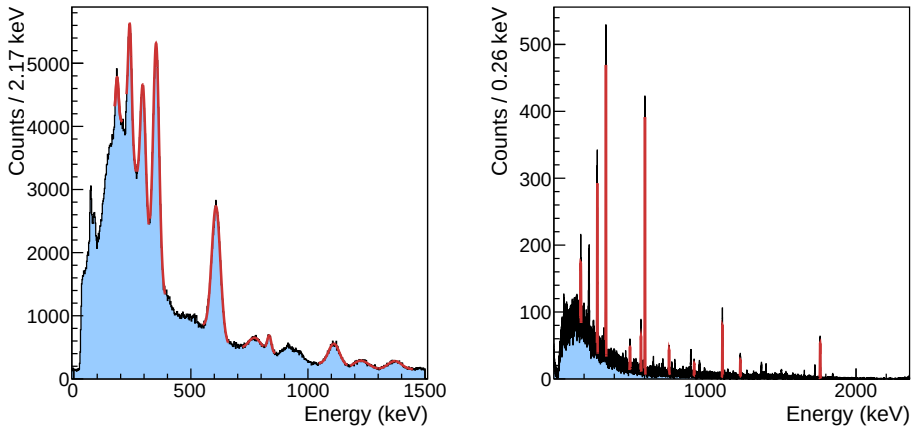

Figure 11: ZrO_2 spectra linked to the NaI(Tl) (left) and HPGe (right) detectors.

4 Radon measurement

The last part of the experiment is dedicated to the determination of the Radon's activity in one room of the "Polo didattico" building; in order to carry out this measurement, *canisters* of activated charcoal were used. In particular, at the beginning of the first session one canister have been weighted ($m = 153.9 \pm 0.1$ g) and then left open in a specific room of the building. At the beginning of the third session (after 48h) the canister was retrieved, sealed and weighted again ($m = 157.7 \pm 0.1$ g); the mass gain is called *water gain* ($wg = 3.8 \pm 0.1$ g) since it's determined by the absorption of water vapor from the activated charcoal. Being the water gain between 1.0 g and 4.0 g, the humidity is conventionally fixed at 50%.

This information, along with the exposure time T_s = 48 h 15 min = 2895 min, is used to determine how many liters of air are filtered by minute from the charcoals; in particular, the *calibration factor* (in l/min) is $CF = CF(2)\frac{AF(T_s)}{AF(2)}$ where $CF(2)$ is the calibration factor for a 48h exposure and $\frac{AF(T_s)}{AF(2)}$ is an adjustment factor that connects the standard CF for a 2 days exposure to the CF for the actual time measurement. In our case, being $T_s \sim 2$ day, we can neglect the AF adjustment and obtain straightforward the calibration factor from Figure 12, namely $CF = 0.107$ l/min for $wg = 3.8$ g.

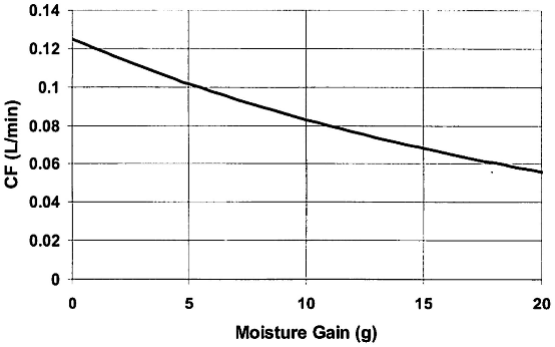

Figure 12: Calibration factor (l/min) as a function of the water gain (g)

To properly evaluate the activity of the exposed canister, one needs to take into account the part of trapped radon that decays before the gamma-measurement. This information can be included in the *decay factor*, being $DF = \exp\left[\frac{-0.693t}{t_{1/2}(^{222}\text{Rn})}\right]$ with $t_{1/2}(^{222}\text{Rn})$ half-life of ^{222}Rn and t the time in minutes from half of the exposure period to when the measurement is performed.

Finally, to perform a correct estimation of the activity one needs to use two other canisters, a non-exposed one for the background measurement and a calibrated one, i.e. of known activity. In particular, the spectra for the three canisters are acquired for 30 min each and are depicted in Figure 13.

Peak (keV)	Probability (%)
242	7.3
295	18.4
352	35.6
609	45.5
768	4.9
1120	14.9

Table 11: List of gamma transitions considered to determine N and E.

Subtracting the background measurement from the spectra, one can obtain the number of events in the major peaks of the ^{222}Rn decay chain for each of the canisters (exposed and calibrated one). In particular, as described in Section 2, the number of photopeak events is obtained through the area of the gaussian fit, subtracting the area of linear background. The gamma transitions and their relative probability are presented in Table 11 [6]. Calling then N the counts for the exposed canister and E the counts for the calibrated one divided by its activity, one can obtain the Radon activity per liter as:

$$RN = \frac{N}{E \cdot T_s \cdot DF \cdot CF}$$

Analyzing the spectra for the germanium detector, the result obtained is: $RN = 0.520$ Bq/l = 520 Bq/m^3. The value is pretty high, considering that "D. Lgs. 31 luglio 2020, n. 101., Art. 12" fixes the maximum average radon activity at 300 Bq/m^3 for workplaces.

One can perform the same analysis with the NaI(Tl) detector despite its low resolution, to check whether the result is compatible with the one previously obtained (that can be considered the true one between the two, given the higher resolution of the former measurement); in particular, the estimation of radon activity is $RN_{\text{NaI}} = 950$ Bq/m^3 which is a really high value. Being incompatible with the previous estimation, we can discharge this last measurement.

[6] Source: http://www.nucleide.org/DDEP_WG/Ra-226D_NT08-059.pdf

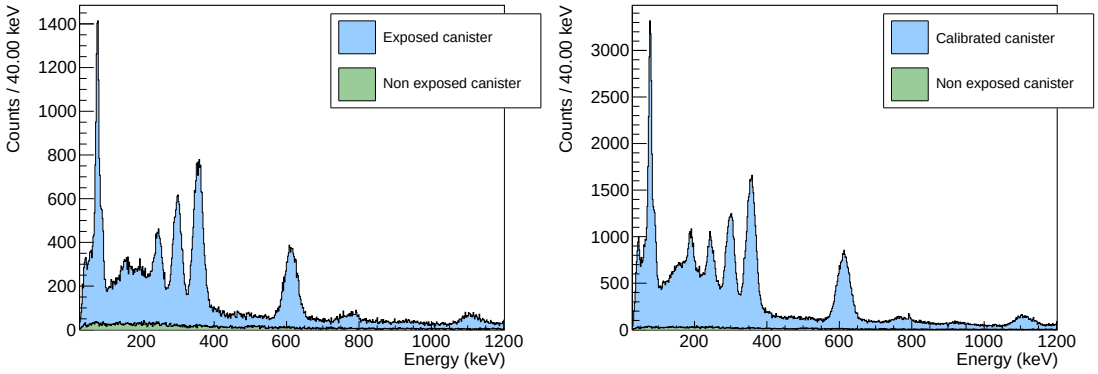

(a) Exposed and non exposed canister, NaI(Tl) (b) Calibrated and non exposed canister, NaI(Tl)

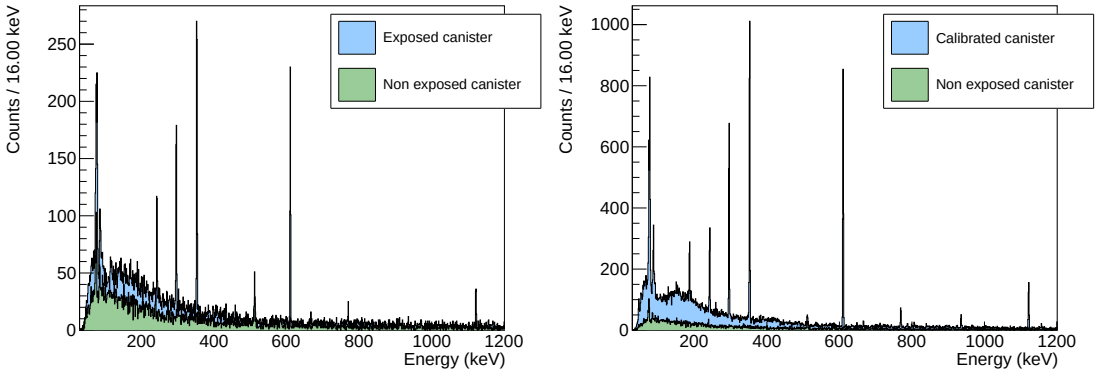

(c) Exposed and non exposed canister, (HPGe) (d) Calibrated and non exposed canister, (HPGe)

Figure 13: Spectra for the different canisters

Autunite sample Lastly, we want to analyze a sample of Autunite (hydrated calcium uranyl phosphate) which, containing Uranium, is expected to present similar peaks to the Radon canister (being ^{238}Ur the precursor of ^{222}Rn). The sample is measured and analyzed as described in Section 3, considering distances $d_{\text{HPGe}} = 75$ mm, $d_{\text{NaI(Tl)}} = 37.5$ mm; the resulting spectra with subtracted background are depicted in Figure 14, while the recognized transition and their relative activity are listed in Table 15.

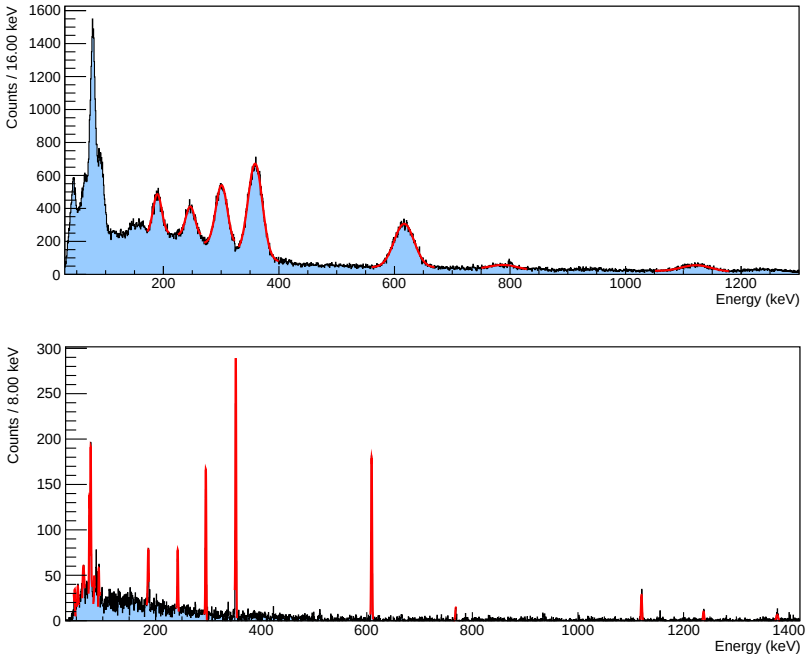

Figure 14: Autunite spectra, NaI (above) HPGe(below)

Energy (keV)	Nuclide	$\mathcal{A}_m$ (Bq/g)
185	^{226}Ra	9.07
242	^{214}Pb	14.1
295	^{214}Pb	15.3
352	^{214}Pb	16.8
609	^{214}Bi	13.6
768	^{214}Bi	21.7
1120	^{214}Bi	19.9

(a) NaI(Tl)

Energy (keV)	Nuclide	$\mathcal{A}_m$ (Bq/g)
47	^{210}Pb	1.99
53	^{214}Pb	12.9
63	^{234}Th	11.1
75	^{214}Pb	8.28
77	^{214}Bi	7.94
84	^{231}Th	1.06
92	^{234}Th	5.65
186	^{226}Ra	4.45

(b) HPGe

Energy (keV)	Nuclide	$\mathcal{A}_m$ (Bq/g)
242	^{214}Pb	9.10
295	^{214}Pb	9.44
352	^{214}Pb	8.77
609	^{214}Bi	8.31
768	^{214}Bi	5.40
1120	^{214}Bi	10.4
1238	^{214}Bi	11.9
1377	^{214}Bi	20.0

(c) HPGe

Figure 15: Transitions found in Autunite and relative activity. The transitions found in the Radon analysis are highlighted.

As expected, all the transitions analyzed for the Radon measurement are present (the ones highlighted). Notice that in the NaI(Tl) spectrum the low energy transitions cannot be recognized due to the low resolution of the detector. Finally, exploiting the activity for each gamma transition, one can obtain the total activity of the sample, namely $\mathcal{A}_m^{\text{NaI(Tl)}} = 111$ Bq/g, $\mathcal{A}_m^{\text{HPGe}} = 136$ Bq/g. The results for the two detectors are quite similar, even though the germanium estimation is higher like for the analysis of Section 3. A possible explanation can be found in the fact that the low energy transitions for the Sodium iodide are not considered for the activity esteem, meaning a lower value for the latter quantity.

5 Conclusions

After the analysis, we can conclude that:

1. the calibration of both the NaI(Tl) and the HPGe detectors was sufficiently accurate, since it did not show any systematic error in the position of the calibrated peaks;
2. the intrinsic efficiency of the detectors trend as function of the energy was characterized thanks to the ^{241}Am, ^{60}Co and ^{152}Eu sources and as a result an exponential fit was operated;
3. the most relevant radionuclides in KCl, Porphyry, ZrO_2, pellet and Autunite samples were identified and the activity was thus estimated;
4. the Radon activity per liter was determined to be $RN = 520$ Bq/m^3, a large value considering the maximum allowed activity in workplaces.